NASA Contractor Report 172393

NASA-CR-172393
19840024713

A Simulation of Remote Sensor Systems and Data Processing Algorithms for Spectral Feature Classification

R. F. Arduini, R. M. Aherron, and R. W. Samms

Information & Control Systems, Incorporated
Hampton, VA 23666

Contract NAS1-16870

July 1984

NASA
National Aeronautics and
Space Administration

Langley Research Center
Hampton, Virginia 23665

24 1 1 RN/NASA-CR-172393

DISPLAY 24/2/1

84N32784*# ISSUE 22 PAGE 3597 CATEGORY 35 RPT#: NASA-CR-172393 NAS 1.26:172393 FR-683110 CNT#: NAS1-16870 84/07/00 54 PAGES

UNCLASSIFIED DOCUMENT

UTTL: A simulation of remote sensor systems and data processing algorithms for spectral feature classification TLSP: Final Report

AUTH: A/ARDUINI, R. F.; B/AHERRON, R. M.; C/SAMMS, R. W.

CORP: Information and Control Systems, Inc., Hampton, Va. AVAIL.NTIS SAP: HC A04/MF A01

MAJS: /*CLASSIFICATIONS/*DATA PROCESSING/*MULTISPECTRAL BAND SCANNERS/* PERFORMANCE PREDICTION/*REMOTE SENSORS/*SIMULATION/*SPECTRAL REFLECTANCE

MINS: / ALGORITHMS/ ATMOSPHERIC EFFECTS/ ATMOSPHERIC SCATTERING/ COMPUTER PROGRAMS/ INSOLATION

ABA: Author

ABS: A computational model of the deterministic and stochastic processes involved in multispectral remote sensing was designed to evaluate the performance of sensor systems and data processing algorithms for spectral feature classification. Accuracy in distinguishing between categories of surfaces or between specific types is developed as a means to compare sensor systems and data processing algorithms. The model allows studies to be made of the effects of variability of the atmosphere and of surface reflectance, as well as the effects of channel selection and sensor noise. Examples of these effects are shown.

ENTER:

ABSTRACT

A computational model of the deterministic and stochastic processes involved in multispectral remote sensing has been developed to evaluate the performance of sensor systems and data processing algorithms for spectral feature classification. Accuracy in distinguishing between categories of surfaces or between specific surface types is used as a criterion for comparing sensor systems and data processing algorithms. The model allows studies to be made of the effects of variability of the atmosphere and of surface reflectance, as well as the effects of channel selection and sensor noise. Examples of these effects are shown.

TABLE OF CONTENTS

LIST OF TABLES

LIST OF FIGURES

LIST OF FIGURES (CONCLUDED)

I. INTRODUCTION

The amount of data generated by a multispectral remote sensor system which is used for global resource monitoring and land use (such as the Landsat Multispectral Scanner or Thematic Mapper) is enormous. One approach to drastically reducing the data transmission and processing load is to design multispectral sensors which are "smart" enough to identify and transmit only the data of interest. Such a smart sensor might be designed to distinguish vegetation from water or bare land and to determine the presence of clouds which obscure the view of the surface. At a higher level of classification, the smart sensor could differentiate between different types of vegetation or soil, e.g., oats and wheat or clay and sand. To accomplish such tasks it is understood that spectral discrimination would have to be augmented by other information in a complete smart sensor system, however, classification of signals according to their spectral differences (or similarities) is fundamental to the smart sensor approach.

This report describes a computational model of the multispectral remote sensing process which was developed to be used as a tool in the study of smart sensor design concepts and data processing algorithms.

The modeling effort was divided into two major tasks: (1) to simulate the radiance at the satellite and its conversion by the sensor into a "signal" and (2) to process these signals so that they may be classified and the accuracy of their classification may be measured. A major objective in this effort was to include a realistic model of the variability of the elements in the remote sensing process. This explicit accounting for the stochastic properties of atmospheric radiative transfer and of surface reflectance and modeling of sensor sensitivity is what makes this model different from most other remote sensing

models (Refs. 1 - 7). This report will describe the model and give a few examples of how the model may be used. First the signal generation is described, followed by a discussion of the signal processing algorithms which have been implemented, including classification algorithms. This is followed by a few results to show the applicability of the model.

II. REMOTE SENSING MODEL

The computational model to simulate the acquisition and classification of multispectral data encountered in remote sensing of the earth's surface is described here. The data acquisition process must account for the solar irradiance, the transfer of radiation through the atmosphere, surface reflection and the sensor's spectral response. Each of these elements may be described by a model which has both deterministic and stochastic components. Variability in the atmospheric attenuation, uncertainty about the physical state of the surface and sensor noise all contribute to the stochastic nature of the signal produced by a remote sensor system and they all affect the performance of a data classification process.

Figure 1 shows schematically the processes included in modeling the generation of signals by the remote sensor and Figure 2 shows the options available for processing the signals. The model actually comprises five programs: STIMULA for stochastic simulation of the signal generation procedures; SCATPLT, HISTPLT, and ELLIP for displaying the signals generated; and BNDARY, RPLPROG, and CLASIFY for processing the signals. These will be discussed below.

A. Signal Generation

Referring to Figure 1 it can be seen that the radiance at the sensor at satellite altitude is the result of a number of processes. Energy from the sun is incident at the top of the atmosphere. In transit to the surface, it may be scattered or absorbed by atmospheric constituents or it may be transmitted unaltered. At the surface, the energy is reflected or absorbed according to some reflection law (which, in general is quite complex) and begins its return trip through the atmosphere, after which it is detected by the sensor and

is converted into a signal.

The signal in the j-th channel of a J-channel multispectral system is given by

$$s_j = \int_0^\infty L(\lambda)\, S_j(\lambda)\, d\lambda \qquad (1)$$

where $L(\lambda)$ is the spectral radiance incident upon the sensor and $S_j(\lambda)$ is the spectral response of the j-th channel. Calculation of the spectral radiance $L(\lambda)$ and the evaluation of the above integral for a large number of surfaces and atmospheric conditions is the purpose of program STIMULA.

The spectral radiance incident on the sensor can be modeled as (Refs. 2 - 4)

$$L = \frac{1}{\pi} (E_o\, T_o\, \mu_o + L_d)\, \rho T + L_p \,, \qquad (2)$$

where

$E_o = E_o(\lambda)$	- solar irradiance at top of atmosphere
$T_o = T_o(\lambda, \tau, \mu_o)$	- atmospheric transmittance along the incidence path
$T = T(\lambda, \tau, \mu)$	- atmospheric transmittance along the exitance path
$L_d = L_d(E_o, \lambda, \tau, \mu_o, \rho, \rho')$	- total downwelling sky radiance
$L_p = L_p(E_o, \lambda, \tau, \mu_o, \mu, \phi, \rho, \rho')$	- path radiance along the path from surface to sensor
$\rho = \rho(\lambda)$	- spectral reflectance of target
$\rho' = \rho'(\lambda)$	- spectral reflectance of background
$\mu_o = \cos\theta_o$	- where θ_o is solar zenith angle
$\mu = \cos\theta$	- where θ is viewing zenith angle

The other parameters are wavelength λ, optical thickness $\tau = \tau(\lambda)$ of the atmosphere,

and azimuth angle ϕ between the plane of incidence and exitance. The component of the total radiance L which is reflected from the surface into the viewing direction is referred to as the beam radiance $L_b = L_b(E_o, \lambda, \tau, \mu_o, \mu, \phi, \rho, \rho')$ and is given by $L_b = L - L_p$. These processes and their implementation in the model are discussed here.

1. Solar Irradiance

The solar irradiance at the top of the Earth's atmosphere is relatively well known (compared to some of the other processes in this model) and although it does vary, it is assumed that its variability is small compared to the others in this system and so is ignored. The data shown in Figure 3 comes from Labs and Neckels (Ref. 8) and is stored in a table in STIMULA. Linear interpolation is used to find the value of irradiance between wavelength grid points.

2. Atmospheric Transmittance

The transmittance of the atmosphere to solar radiation in the visible and near infrared wavelength regions (.2 - 2 μm) is reduced primarily by Rayleigh scattering, aerosol extinction and absorption by water vapor, carbon dioxide and ozone. The atmospheric transmittance over the incidence path is given by

$$T_o = e^{-\tau/\mu_o}$$

and over the exitance path by

$$T = e^{-\tau/\mu}$$

where τ is the optical thickness and μ, μ_o are the cosines of the solar and viewing zenith angles respectively. The optical thickness τ is given by

$$\tau(\lambda) = \sum_{i=1}^{n} \alpha_i(\lambda)\, x_i \qquad (3)$$

with $\alpha_i(\lambda)$ being the spectral attenuation coefficient of the i-th atmospheric constituent and x_i the associated attenuator amount. The constituents referred to here are those mentioned above: total molecular content, water vapor, carbon dioxide and ozone. The spectral coefficients for these absorbers were taken from the AFGL LOWTRAN 5 model (Ref. 9).

To simulate the effects of atmospheric variability, it is assumed that the attenuator amounts in Eq. (3) are random variables with a known mean $\bar{x}_i$ and standard deviation σ_i. Although it is not necessary for the simulation, it is convenient to assume that each of the attenuator amounts has a Gaussian distribution, thereby enabling use of an on-line random number generator to simulate random variations in the absorber amounts. The random number generator produces pseudo-random numbers having a normal (Gaussian) distribution with zero mean and unit variance. To simulate a particular value of the attenuator amount, the random variable x_i is computed by

$$x_i = \bar{x}_i + q\,\sigma_i$$

where q is the random number. The mean values $\bar{x}_i$ and standard deviations σ_i are inputs to the program and are given in Table 1.

3. Multiple Scattering

To include the effects of multiple scattering by the atmosphere it was decided to use the program RADMOD, which was developed by Turner, et. al., (Refs. 2 - 4) and which was obtained from the Environmental Research Institute of Michigan. The program and its auxiliary program VISTAU (used to calculate the required optical depth properties) were adapted to fit the needs of this simulation. RADMOD forms the basis for the radiative transfer calculations. It provides the capability to compute the diffuse radiance and the path radiance

(L_d and L_p in Eq. (2), respectively) which result from multiple scattering process.

The single scattering albedo (which determines the relative amount of attenuation due to scattering alone) is related to the relative humidity and visual range. Variability in the multiple scattering simulation therefore was accomplished by fixing the visual range and then varying the relative humidity in the same manner as described above for the atmospheric absorbers.

The scattering phase function used here is one of several supplied with the RADMOD program by ERIM. All of the simulations run thus far have employed a phase function with properties typical of a weakly absorbing continental aerosol. Data is available to simulate both continental and marine aerosols with a range of absorbing properties from no absorption to "strong" absorption.

Table 1 summarizes the parameters used in the simulation.

4. Surface Reflectance

Since targets on the surface are to be identified and classified according to their spectral reflectance characteristics, it is clearly important for the simulated spectral reflectances and their variabilities to be realistic. The reflectance properties of natural surfaces are not only a function of wavelength but also of many other factors such as the direction of both the incident and reflected rays, the moisture content for soils and the stage of growth for vegetation. These factors plus the difficulties involved in making measurements of natural surfaces make it very difficult to assemble a representative collection of spectral reflectance data. It is particularly difficult to find information about the typical variability of spectral reflectances (except for some vegetation) and about their spatial distribution or probability of occurrence. Furthermore, it is awkward to deal with spectral reflectance data that

often cover only part of the wavelength region of interest.

The spectral reflectance data implemented thus far is limited to two sets: (a) one for vegetation, bare land, water, snow and clouds in the 0.4 to 2.0 μm region, and (b) an expanded set for vegetation and bare land for the more limited 0.4 to 1.0 μm region. It is also assumed that all reflectances are Lambertian.

To simulate the effects of surface reflectance variability, the reflectance of a particular target surface is modeled by

$$\rho(\lambda) = \rho_o(\lambda)\, e^{-x_o \beta_o(\lambda)} \quad , \tag{4}$$

where $\rho_o(\lambda)$ and $\beta_o(\lambda)$ are deterministic functions which are characteristic of the surface, and x_o is the standard normal random variable with mean = 0. and variance = 1. For each surface the parameters $\rho_o(\lambda)$ and $\beta_o(\lambda)$ are estimated from empirical reflectance data using the relationships (Ref. 10).

$$\rho_o(\lambda) = \frac{\langle \rho(\lambda) \rangle}{\left[\dfrac{\sigma_\rho^2(\lambda)}{\langle \rho(\lambda) \rangle^2} + 1 \right]^{\frac{1}{2}}} \tag{5}$$

and

$$\beta_o(\lambda) = \left\{ \ln \left[\frac{\sigma_\rho(\lambda)}{\langle \rho(\lambda) \rangle^2} + 1 \right] \right\}^{\frac{1}{2}} \tag{6}$$

where

$$\sigma_\rho^2(\lambda) = \left\langle \left[\rho(\lambda) - \langle \rho(\lambda) \rangle \right]^2 \right\rangle .$$

The model given by Eq. (5) has been shown to be approximately representative of the reflectance variability of vegetation canopies (Ref. 11) and does indeed produce a random family of reflectances which agrees qualitatively with selected

data sets. This model is also used for the reflectance variability of other targets simply because there are insufficient data in the literature to suggest another model. Table 2 summarizes the categories and substances used in this work as well as the (assumed) standard deviation σ_ρ of their reflectance variability. Figure 4 illustrates the (expected) mean values $\langle\rho(\lambda)\rangle$ of the spectral signatures and Figure 5 shows the simulated variability of two of these signatures.

The mean spectral reflectances used for vegetation represent in situ measurements. The curves for crops were obtained mostly from Leeman, et. al., (Ref. 12) and Suits and Safir, (Ref. 13) and the curves for forests from Vlcek, (Ref. 14). The associated variables fall roughly within the range of variabilities reported by Collins, (Ref. 15) and Duggin, (Ref. 16). Rao, et. al., (Ref. 17) who report on the reflectance variability of crops, incorporate an unspecified correction for atmospheric effects, so that their results are not well suited for simulation studies; and Vlcek, (Ref. 14) who reports on the reflectance variability of forests, gives an average variability of reflectance that is only ±5 percent of the mean reflectance, which is much lower than the variability reported by Collins, (Ref. 15) and Duggin, (Ref. 16).

The spectral reflectance curves for bare land were obtained mostly from Condit, (Ref. 18) and the Infrared Handbook, (Ref. 19). The mean spectral reflectance curves shown in Figure 4 are the averages of the wet and dry reflectance curves given by Condit, and the variables of the spectral reflectances were obtained by using the wet and dry reflectance curves as the mean reflectance plus or minus 1 standard deviation.

The variability for water was obtained from the water reflectance variations for varying amounts of chlorophyll, as given in the Infrared Handbook,

(Ref. 10). The spectral reflectance for snow was obtained from data reported by O'Brien and Munis, (ref. 20) with data for the 0.4 to 0.6 μm spectral region added from Reference 19. The variability represents the range of reflectances obtained from samples with different thermal histories. The spectral reflectance curves for ice clouds with different atmospheric thicknesses were obtained from the analytical results of Novosel'tsev, (Ref. 21) and the experimental results of Zander, (Ref. 22). A standard deviation in reflectivity of 0.1 was chosen for clouds based on data presented in Kondratyev, (Ref. 23).

All of this reflectance data is stored and maintained in a data base which employs random access files. This feature provides quick access to any particular subset of the data. The data base programs allow several options which include the ability to add new data, to list the titles of all the data currently stored, and to update particular data sets.

5. Signal Computation

The spectral radiance at the top of the atmosphere as produced by the above model is shown in Figure 6. Three visual ranges and two solar zenith angles are shown with oats as target and bare moist soil as background. The variability of this radiance field is shown in Figure 7. In Figure 7(a) target and background reflectance values are kept constant, and only the atmospheric absorber amounts are varied; in Figure 7(b) both surface and atmosphere are permitted to vary.

The sensor converts the radiance L into the signal vector $\underline{s}$ with components s_j. To facilitate comparison of signals obtained with different spectral response shapes, it is convenient to normalize this conversion by the integrated spectral response of the sensor and model the signal component s_j as

$$s_j = \int_0^\infty L(\lambda)\, S_j(\lambda)\, d\lambda \Big/ \int_0^\infty S_j(\lambda)\, d\lambda + n_j, \qquad (7)$$

where $S(\lambda)$ is the spectral response, n is the normalized electronic noise, and the subscript j denotes the jth channel. The electronic noise n is characterized as a normal random variable with mean = 0 and variance σ_n^2.

Three sets of sensor channels are used in this simulation. They include the U.S. Landsat Thematic Mapper (TM), (Ref. 24), the French System Probatoire d'Observation de la Terre (SPOT), (Ref. 25) and those proposed by the Russian scientists Kondratyev, Vasilyev and Ivanyan (KON), (Ref. 26). Their spectral responses are shown in Figure 8. The TM and SPOT responses are based on sensor response measurements, whereas the shapes of the KON responses are somewhat arbitrarily selected for the intervals recommended by Kondratyev. In addition to these channels, the TM has two other channels (centered at 2.24 and 11.5 μm) and the SPOT has one other channel (panchromatic, 0.5 to 0.7 μm).

Table 3 lists sensitivity characteristics of the TM. The TM signal-to-noise ratios (SNR) are given by Salomonson, (Ref. 24) for specified surface reflectances ρ and solar incidence angles θ_o; however, the atmospheric state was not specified, and thus had to be chosen arbitrarily for our simulation.

6. Program Structure for STIMULA

The basic structure of program STIMULA is shown in Figure 9. The program consists of a driver program, MAIN, which invokes the subroutines which initialize parameters, assemble data and perform the calculations. The principal subroutine SIMULA drives the actual simulation.

Subroutines CALPHA (which assembles the atmospheric attenuation coefficients), SOLARI (which sets up the solar irradiance) and SREFL (which reads the surface reflectance data) all handle data which are stored in tables as functions of wavelength. To access data values at spectral grid points required by the simulation, it was decided to use average values of the spectral functions

over the appropriate spectral bins. To do so required an integration which was performed in subroutine INTGRT using a Simpson's rule integration method.

Subroutine PFINPT reads in the single scattering phase function data supplied with the RADMOD software.

Subroutine SETRAN is used to initialize the random number generator GETRAN.

Subroutine NCVRCND is used to read the input data to set up a particular simulation. AEROSOL assigns a value of the aerosol amount based upon visual range read in NCVRCND.

Once all the arrays are assembled, subroutine SIMULA is called. First ZERSTS is called to zero out the necessary arrays. Then the target reflectance and the reflectance variability parameters are read using SREFL and RFLPRM respectively. Subroutine PERTRB is used to generate all of the random variables described above. Subroutine CTAU is used to calculate the atmospheric optical thichness given by Eq. (3). Subroutine RFLRND is used to evaluate the reflectance according to Eq. (4). Subroutine GENCND is used to calculate the single scattering albedo and sun-surface-viewing geometry factors. RADMOD is then called to calculate the radiance at the sensor which is then passed to CSIGNL which calculates the signal in each channel of the sensor system to provide the signal vectors. These signal vectors are then stored and used as input to the signal processing programs which are described below.

B. Signal Processing

Once the simulated signal vectors have been computed, a number of options are available (see Figure 2). The J-dimensional signal vectors, whose elements are the values of the signals in each channel of the system, are generated a large number of times (100), thus, allowing the parameters to vary sufficiently so that the stochastic nature of the simulation may be studied. Among the options which have been implemented are programs to display two-dimensional scatter

plots of the signals in the signal space (SCATPLT), ellipse plots to characterize the variation and covariance between channels (ELLIP) and histograms to show the distribution of signal values about the mean (HISTPLT). These all provide means by which the signal statistics (mean values, standard deviations and covariances between channels) can be studied as viewing conditions change. Examples of these plots are shown in Figures 10 - 12.

The ellipse plots drawn by program ELLIP are two-dimensional projections of J-dimensional, one-sigma covariance ellipsoids onto the plane shown. These ellipses depict the relative size and orientation of the signal scatter, but they do not actually indicate the number of measurements contained within their areas.

1. Analysis of Stochastic Processes

The spectral radiance $L(\lambda)$ that reaches the sensor is modeled as a stochastic process whose value at each wavelength λ depends upon a number of random variables associated with both the atmosphere and surface. Letting the operation $E\{\bullet\}$ denote the expectation (average) taken over the ensemble of all possible radiances associated with a particular surface, the mean $\langle L(\lambda)\rangle$ and autocovariance $C(\lambda,\lambda')$ of the radiance can be expressed as

$$\langle L(\lambda)\rangle = E\{L(\lambda)\} \tag{8}$$

and

$$C_L(\lambda,\lambda') = E\{[L(\lambda) - \langle L(\lambda)\rangle] \bullet [L(\lambda') - \langle L(\lambda')\rangle]\} \quad . \tag{9}$$

Likewise, the signal vector $\underline{s}$ resulting from measuring the radiance may be treated as a multivariate random variable whose mean $\underline{r}$ and covariance $\underline{C}$ have components denoted by

$$r_j = E\{s_j\} \qquad \text{and}$$

$$\sigma_{jj'} = E\{(s_j - r_j)(s_{j'} - r_{j'})\} \quad .$$

where both j and j' take on the value 1, 2, ..., J, and J is the total number of channels. The signal conversion process is assumed to be linear, and the radiance field and electronic gain and noise are assumed to be independent of each other. The reference patterns can then be computed as

$$r_j = \int_0^\infty \langle L(\lambda) \rangle \, S_j(\lambda) \, d\lambda \tag{10}$$

and

$$\sigma_{jj'} = \int_0^\infty \int_0^\infty C_L(\lambda,\lambda') \, S_j(\lambda) \, S_{j'}(\lambda') \, d\lambda \, d\lambda' + \sigma_n^2 \, \delta_{jj'} \tag{11}$$

where $\langle L(\lambda) \rangle$ and $C_L(\lambda,\lambda')$ are the mean and autocovariance of the radiance as given by Eq. (3).

It is often advantageous to ratio the signal vector to reduce effects of radiance variations that tend to result more from changes in atmospheric conditions and lighting and viewing geometry than from changes in the spectral reflectance properties that are relied upon to discriminate between various targets. One of the more common approaches for ratioing the signal vector $\underline{s}$ is to divide each component of $\underline{s}$ by the sum of the components; that is, the normalized vector components s_j, are computed as

$$s_j' = \frac{s_j}{\sum_{j=1}^{J} s_j} \tag{12}$$

This ratioing process is a coordinate transformation which maps the J-dimensional feature space into a (J-1)-dimensional feature space; that is, ratioing reduces the dimensionality of the multispectral signal by one.

2. Decision Rules

The function of decision rules in pattern recognition tasks is to assign the signal vector $\underline{s}$ to selected classes. These classes may be groups of similar targets (i.e., categories), or they may be very restrictive sets of individual targets. The distinction is denoted here by the terminology: categorization referring to an assignment to a group of similar targets (i.e., soil, vegetation, cloud, etc.) and identification referring to assignment to a particular target type (e.g., wheat, oats, clay, etc.).

The usual objective in classifying data is to maximize the conditional probability $P(c_i^m/s)$ that the selected target c_i^m is the true identification, given that measurements of this target generate signal vectors with certain characteristics denoted by the feature vector $\underline{s}_i$. This objective is realized by the simple Bayes decision rule which assigns the signal vector $\underline{s}$ to a target c_i if and only if

$$P(c_{i'}^{m'}/\underline{s}) \geq P(c_i/\underline{s}) \quad , \tag{13}$$

$$m = 1, 2, \ldots, M \quad ; \quad i = 1, 2, \ldots, I_m$$

where M is the total number of categories, and I_m the total number of target types in category m.

a. Boundary Approximation Method

Targets belonging to a particular category often have some common spectral reflectance properties which tend to distinguish them from targets belonging to other categories. For example, all vegetations have a sharp increase in reflectance at around 0.7 μm, beyond the strong absorption bands of chlorophyll. This feature is what characterizes vegetation from other surface types.

If sensor channels are selected appropriately, these features may produce

a distribution of original vectors $\underline{s}$ which will tend to cluster in the J-dimensional feature space so that they can (hopefully) be categorized simply by their location in the feature space. This is the approach taken in developing the boundary approximation method (BAM). In this decision rule the regions of the J-dimensional feature space where signal vectors for specific targets tend to fall are delineated by boundaries. The determination of favorable boundaries for categorizing signal vectors as either bare land, vegatation, water, snow or clouds and to analyze the sensitivity of these boundaries to changes in imaging conditions is one application of this model.

b. Mean Square Distance and Maximum Likelihood Classification

The conditional probability $P(c_i^m/\underline{s})$ used by the Bayes decision rule in Eq. (13) and the conditional probability $P(\underline{s}/c_i^m)$ of the signal vector distribution for target c_i^m are related by

$$P(c_i^m/\underline{s})\ P(\underline{s}) = P(\underline{s}/c_i^m)\ P(c_i^m) \quad , \tag{14}$$

where $P(\underline{s})$ is the probability of occurrence of signal vector $\underline{s}$, and $P(c_i^m)$ is the probability of occurrence of data having the true identification c_i^m. According to Eq. (13), the Bayes decision rule assigns the signal vector $\underline{s}$ to target $c_i^{m'}$, whenever the conditional probability $P(c_i^m/\underline{s})$ is greater for $\underline{r}_i^{m'}$ and $c^{m'}{}_i$, than for all other $\underline{r}_i^m$ and $\underline{c}_i^m$, m = 1, 2, ..., M, and i = 1, 2, ..., I_m. The probabilities $P(\underline{s})$ and $P(c_i^m)$ are generally not known *a priori*. Thus, classification of remotely sensed multispectral data usually reduces in practice to the maximum likelihood (MLH) decision rule which assigns the target $c_i^{m'}$, to any signal vector $\underline{s}$ if and only if

$$P(\underline{x}/c_i^{m'},) \geq P(\underline{s}/c_i^m) \quad ,$$

$$m = 1, 2, \ldots, M, \quad i = 1, 2, \ldots, I_m,$$

The MLH and simple Bayes decision rule are related by the probability of occurrence of data having true identification c_i^m, denoted here by $P(c_i^m)$, as follows:

$$P(c_{i'}^{m'}/\underline{s}) \geq P(c_i^m/\underline{s}) \text{ IF AND ONLY IF } P(\underline{s}/c_{i'}^{m'})\ P(c_{i'}^{m'}) \geq P(\underline{s}/c_i^m)\ P(c_i^m)$$

$$m = 1, 2, \ldots, M, \quad i = 1, 2, \ldots, I_m.$$

The relative occurrences of targets of interest in typical remote sensing tasks are usually unequal and, unfortunately, also unknown. Because of this lack of information, we assume that the a priori probabilities of occurrence of the targets are equal, in which case the MLH and simple Bayes decision rules are identical. This assumption obviously imposes constraints on the conclusions that can be drawn from predictions of classification accuracy.

It is common in MLH decision processes to characterize the statistical distribution of the reference (or training) data by an analytical probability density function (PDF) with only a few parameters in order to reduce storage requirements. The most frequently used function is the J-dimensional multivariate normal or Gaussian PDF which is given by the expression

$$P(\underline{s}_i/c_i^m) = \frac{1}{(2\pi)^{J/2} \left|\underline{C}_i^m\right|^{\frac{1}{2}}} \exp\left[-\frac{1}{2}\ (\underline{s} - \underline{r}_i^m)^t\ (\underline{C}_i^m)^{-1}\ (\underline{s} - \underline{r}_i^m)\right] \qquad (15)$$

where $\underline{r}_i^m$ and $\underline{C}_i^m$, respectively, are the mean vector and covariance matrix for target c_i^m and are given by

$$\underline{r}_i^m = \int \underline{s}\ P(\underline{s}/\underline{C}_i^m) \prod_{j=1}^{J} ds_j \qquad (16)$$

and

$$\underline{C}_i^m = \int (\underline{s} - \underline{r}_j^m)\ (\underline{s} - \underline{r}_j^m)^t\ P(\underline{s}/\underline{C}_i^m) \prod_{j=1}^{J} ds_j \qquad (17)$$

To avoid the computational expense of evaluating the exponent in Eq. (15), an equivalent classification procedure can be used which minimizes $-\ln P(\underline{s}/c_i^m)$. This procedure is realized by the so-called MLH (or Gaussian) classifier which assigns $\underline{s}$ to c_i^m if and only if

$$(\underline{s} - \underline{r}_{i'}^{m'})^t \, (\underline{C}_{i'}^{m'})^{-1} \, (\underline{s} - \underline{r}_{i'}^{m'}) + \log_e \left|\underline{C}_{i'}^{m'}\right| \leq (\underline{s} - \underline{r}_i^m)^t \, (\underline{C}_i^m)^{-1} \, (\underline{s} - \underline{r}_i^m) + \log_e \left|\underline{C}_i^m\right| , \tag{18}$$

$m = 1, 2, \ldots, M, \quad i = 1, 2, \ldots, I_m.$

The number of computations and storage required for the MLH classifier is further reduced by disregarding the statistical distribution of the signal so that the covariance matrix $\underline{C}$ reduces to the identity matrix. The resulting mean-square distance (MSD) classifier assigns $\underline{s}$ to c_i^m if and only if

$$(\underline{s} - \underline{r}_{i'}^{m'})^t \, (\underline{s} - \underline{r}_{i'}^{m'}) \leq (\underline{s} - \underline{r}_i^m)^t \, (\underline{s} - \underline{r}_i^m), \tag{19}$$

$m = 1, 2, \ldots, M \; ; \; i = 1, 2, \ldots, I_m.$

The improvement in classification accuracy that can be attained by the MLH classifier over the MSD classifier depends on two factors: the extent to which the statistical distribution of the reference data is representative of all acquired data for the selected targets; and the fit of the assumed (Gaussian) statistical distribution of the signal for each target (Ref. 27). It is also conceivable that the added expense of performing MLH classification may outweigh the increase in accuracy over the simpler MSD classification. This model has been designed to examine these types of questions.

3. Implementation of Decision Rules

STIMULA simulates an orbiting multispectral sensor system which generates

pseudo-random observations (i.e., signal vectors) from a nadir-looking sensor at the top of the atmosphere. These observations are either assembled as training sets for the reference library or classified using the BAM, MSD, and MLH decision algorithms. The assembly of training sets and the assessment of classification accuracy are both based upon a total of 100 observations per target. Computations with larger numbers of observations (e.g., 400) per target did not significantly change the results (typically only by about 1 percent). The programs BNDARY, RPLPROG and CLASIFY which implement these tasks are described below.

a. BNDARY

Program BNDARY is used to perform feature categorization of signals output from STIMULA by the boundary approximation method (BAM). The boundaries between regions of planes in the signal space are straight lines, and so the parameters specifying the boundaries are the slopes and intercepts of the lines. These parameters are variables in BNDARY and can be adjusted to achieve the maximum accuracy.

The boundaries shown by dashed lines in Figure 11 were selected to divide the signals into their five categories (i.e., vegetation, bare land, water, snow and clouds) with approximately equal consideration for the two most extreme imaging conditions considered in this computational experiment. A tradeoff implicit in this compromise between imaging conditions is illustrated in Figure 13; which shows the variation in discrimination accuracy with changes in the threshold boundary which divides vegetation, land and water from snow and clouds. This type of analysis can be accomplished routinely using BNDARY.

b. RPLPROG

As discussed above, classification by the MSD or MLH schemes requires the computation of discriminant functions which govern the classification process.

To compute the discriminant functions requires repeated use of the mean signal vectors $\underline{r}$ and the covariance matrices $\underline{C}$. These quantities are stored in what is called the "reference pattern library". It seems reasonable to assume that in practice, the reference pattern library would be generated under clear sky conditions and so in simulations done to date, the reference patters were calculated using signals simulated under the clearest conditions, namely V=55 km. RPLPROG uses 100 signals for each of the surfaces in the library to generate and store reference patterns comprising the following: the mean signal vectors $\underline{r}_i$, the covariance matrices, their inverses and their determinants, $\underline{C}_i$, $\underline{C}_i^{-1}$, and $|\underline{C}_i|$ respectively. These can then be accessed by the classification program CLASIFY for use in the MSD and MLH algorithms.

c. CLASIFY

Program CLASIFY is used to perform feature identification of multispectral signals by both the MSD and MLH algorithms. Inputs to the program are the signal vectors generated by STIMULA and the reference pattern libraries generated by RPLPROG. Classification accuracy, the fraction of all classifications done correctly, is the output. Since the "true" identification of the signal is known before classification takes place, the calculation of the accuracy is trivial.

Classification by MSD amounts to calculating the "distance" in signal space between the point specified by the signal being classified and each of the mean signals in the reference library and assigning the "unknown" signal to the class for which the distance is a minimum.

Classification by MLH requires the computation of a probability density function for each of the surfaces in the reference library and makes the classification based on the surface which yields the largest probability density.

III. SAMPLE APPLICATIONS

The model described in this report was deisgned to be used in studying smart sensor design concepts. This section of the report gives a few examples of the types of studies which may be performed with this model. A measure of the performance of a smart sensor would be the accuracy with which it classifies specific targets or types of targets. Therefore, the examples shown here display either categorization or classification accuracy as a function of the variable of interest for a number of different conditions. All of the simulations are for a downward looking sensor at the top of the atmosphere. Reference patterns were calculated under the clearest of conditions simulated, i.e., visual range of 55 km and solar zenith angle of 30^{o}.

Figure 14 shows the feature categorization accuracies attained with the BAM using three TM channels centered at 0.67, 0.84, and 1.68 μm respectively. The boundaries employed are those shown in Figure 11.

Figures 15 to 17 present classification results using the MSD and MLH classification schemes. Figure 15 compares the three sets of channels, TM, SPOT, and KON and classification schemes themselves; Figure 16 shows the effects of an additional channel; and Figure 17 shows the effects of simulated noise. For further discussion of all these results see Huck, et. al., (Ref. 28). These are typical examples of the type of studies which are possible by employing this model.

IV. CONCLUDING REMARKS

The computational model described in the report has been designed to be used as a tool in evaluating the performance of potential remote sensor concepts. Such evaluations are useful in developing smart sensors to reduce data processing requirements. The program allows for studies of the variability of atmospheric attenuation processes and surface reflectance and the effects of these variabilities in the performance of multispectral remote sensor systems. Data processing algorithms and their performance in classifying simulated signals may also be examined systematically as a function of the variable elements of the model.

The model is limited by a lack of representative models of the spatial distribution or probability of occurrence of surface and cloud targets and the spectral, angular and temporal variability of their reflectance. Nevertheless, the computational model presented here provides a useful tool for assessing the performance of potential remote sensor concepts.

REFERENCES

1. Malila, W. A., Crane, R. B., Omarzu, C. A., and Turner, R. E., "Studies of Spectral Discrimination", NASA CR-134181, 1971.

2. Turner, R. E., "Atmospheric Effects in Remote Sensing", Remote Sensing of Earth Resources, Shahroki, F., ed., University of Tennessee Space Institute, Vol. II, 1973.

3. Turner, R. E., "Atmospheric Effects in Multispectral Remote Sensor Data", NASA CR-141863, 1975.

4. Turner, R. E., "Elimination of Atmospheric Effects from Remote Sensor Data", Proc. Twelfth International Symposium on Remote Sensing of the Environment, II, 1978.

5. Landgrebe, D. A., Biehl, L. L., and Simmons, W. R., "An Empirical Study of Scanner System Parameters", IEEE Trans. on Geoscience Electronics, GE-15, 1977.

6. Kondratyev, K. Ya., Grigoryev, A. A., and Pokrovskiy, O. M., "Information Content of the Data Obtained by Remote Sensing of the Parameters of the Environment and the Earth's Resources from Space", Izdatel'stvo Leningradskogo Universiteta 17, NASA TT F-16435, 1975.

7. Kondratyev, K. Ya., Beliavsky, A. I., Pokrovsky, O. M., "Possibilities of Optimal Planning of Multipurpose Survey from Space", Proc. Thirteenth International Symposium on Remote Sensing of the Environment, 1979.

8. Smith, E. V. P., and Gottlieb, D. M., "Solar Flux and It's Variations", Space Science Reviews, 16, 1974.

9. Kneizys, F. X., et al., "Atmospheric Transmittance/Radiance Computer Code LOWTRAN 5", AFGL-TR-80-0067, Environmental Research Papers, No. 697, 1980.

10. Huck, F. O., et al., "Computational Modeling for the Study of Multispectral Sensor System and Concepts", Optical Engineering, 21, 1982.

11. Park, J. K., and Deering, D. W., "Relationships between Diffuse Reflectance and Vegetation Canopy Variables based on the Radiative Transfer Theory", NASA TM-82067, 1981.

12. Leeman, V., Earing, D., Vincent, R. K., and Ladd, S., "The NASA Earth Resources Spectral Information System: A Data Compilation", NASA CR-115757, 1971.

13. Suits, G. H., and Safir, G. R., "Verification of a Reflectance Model for Mature Corn with Applications to Corn Blight Detection", Remote Sensing of the Environment, 2, 1972.

14. Vleck, J., "Difficulties in Determining Meaningful Spectral Signatures of Forest Tree Canopies", Proc. Symposium on Remote Sensing and Photo Interpretation, Vol. II, 1974.

15. Collins, W., "Remote Sensing of Crop Type and Maturity", Photogrammetric Engineering and Remote Sensing, 1978.

16. Duggin, M. J., "On the Natural Limitations of Target Differentiation by Means of Spectral Discrimination Techniques", Proc. Ninth International Symposium on Remote Sensing of the Environment, 1974.

17. Rao, V. R., Branch, E. J., and Mack, A. R., "Crop Discriminability in the Visible and Near Infrared Regions", Photogrammetric Engineering and Remote Sensing, 1978.

18. Condit, H. R., "The Spectral Reflectance of American Soils", Photogrammetric Engineering, 1970.

19. Wolfe, W. L., and Zissis, G. J., The Infrared Handbook, Environmental Research Institute of Michigan, 1978.

20. O'Brien, H. W., and Munis, R. H., "U. S. Army Cold Regions Research and Engineering Laboratory Research", Report 332, 1975. Also in The Infrared Handbook, by Wolfe and Zissis.

21. Novosel'tsev, Ye. P., "Spectral Reflectivity of Clouds", NASA TT-F-328, 1965.

22. Zander, R., "Spectral Scattering Properties of Ice Clouds and Hoarfrost", Journal of Geophysical Research, 1966.

23. Kondratyev, K. Ya., ed., Radiation Characteristics of the Atmosphere and the Earth's Surface, Amerind Publishing Co. Pvt. Ltd., New Delhi, 1973.

24. Salomonson, V. V., "Landsat D, A Systems Overview", Proc. Twelfth International Sympsoium on Remote Sensing of the Environment, 1978.

25. Begni, G., "Selection of the Optimum Spectral Bands for the SPOT Satellite", Colloquim on Spectral Signatures of Ground Objects, Avignon, September 1981. Translated by P. N. Slater.

26. Kondratyev, K. Ya., Vasilyev, O. G., and Ivanyan, C. A., "On the Optimum Choice of Spectral Intervals for Remote Sensing of Environment from Space", Remote Sensing of Earth Resources, Shahroki, F., ed., University of Tennessee Space Institute, Vol. II, 1973.

27. Haralick, R. M., "Automatic Remote Sensor Image Processing" Digital Picture Analysis, Rosenfeld, A., ed., Springer-Verlag, 1976.

28. Huck, F. O., Davis, R. E., Fales, C. L., Aherron, R. M., Arduini, R. F., and Samms, R. W., "Study of Remote Sensor Spectral Responses and Data Processing Algorithms for Autonomous Feature Classification", to be published, Optical Engineering, 1984.

TABLE 1. SUMMARY OF PARAMETERS USED IN SIMULATION

PARAMETER	SYMBOL	VALUES	VARIABILITY
GEOMETRY			
SOLAR ZENITH ANGLE	θ_o	30^o, 40^o	---
NADIR VIEWING ANGLE	θ	0^o	---
RELATIVE AZIMUTH	ϕ	100^o	---
SURFACE PROPERTIES			
TARGET REFLECTANCE	ρ_t	see Fig. 4	see Table 2
BACKGROUND REFLECTANCE	ρ_b	see Fig. 4	and Fig. 5
ATMOSPHERIC PROPERTIES			
MOLECULAR OXYGEN BURDEN	X_{O_2}	1.71 km STP	0.13 km STP
WATER VAPOR BURDEN	X_{H_2O}	1.14 cm^{-1}	0.36 cm^{-1}
CARBON DIOXIDE BURDEN	X_{CO_2}	8.01 atm cm	0.24 atm cm
OZONE	X_{O_3}	0.34 atm cm	0.12 atm cm
RELATIVE HUMIDITY	RH	0.40	0.20
SURFACE PRESSURE	P_o	1013 mb	---
VISUAL RANGE	V		
"CLEAR"		55 km	---
"INTERMEDIATE"		33 km	---
"HAZY"		14 km	---

TABLE 2. TARGETS AND THE ASSUMED STANDARD DEVIATION OF THEIR REFLECTANCE

(a) WAVELENGTH REGION: 0.4 - 2.0 μm

CATEGORY	SUBSTANCE	CODE	STANDARD DEVIATION OF REFLECTANCE σ_ρ
I. VEGETATION	COTTON	V1	0.1
	TOBACCO	V2	0.1
	BEAN	V3	0.1
	OATS	V4	0.1
	PINE	V5	0.1
II. BARE LAND	BARE MOIST SOIL	L1	0.13
	DRY SAND	L2	0.1
	LOAM, 1% WATER	L3	0.11
	GNEISS	L4	0.1
III. WATER	SEA WATER	W	0.06
IV. SNOW	SNOW, 14 HOURS	S1	0.08
	SNOW, 44 HOURS	S2	0.08
	SNOW, 70 HOURS	S3	0.08
V. CLOUD	ICE CLOUD, $\tau = 128$*	C1	0.1
	ICE CLOUD, $\tau = 16$	C2	0.1
	ICS CLOUD, $\tau = 8$	C3	0.1
	ICE CLOUD, $\tau = 4$	C4	0.1

*τ is optical thickness

TABLE 2. TARGETS AND THE ASSUMED STANDARD DEVIATION OF THEIR REFLECTANCE. (CONCLUDED)

(b) WAVELENGTH REGION: 0.4 - 1.0 μm

CATEGORY	SUBSTANCE	STANDARD DEVIATION OF REFLECTANCE σ_ρ
I. VEGETATION	WHEAT	0.1
	BEAN	0.1
	BARLEY	0.1
	OATS	0.1
	CORN	0.1
	RED SPRUCE	0.1
	BALSAM FIR	0.1
	COTTONWOOD	0.1
	ASPEN PINE	0.1
	WHITE PINE	0.1
II. BARE LAND	BARE SOIL	0.13
	PEDOCAL, OHIO	0.11
	PEDOCAL, NEBRASKA	0.02
	PEDOCAL, OKLAHOMA	0.1
	CLAY, MISSOURI	0.06
	QUARTZ SAND, OREGON	0.14
	CHERNOZEM, NEBRASKA	0.13
	PEDALFER SILT, ARKANSAS	0.11
	RED QUARTZ AND CALCITE SAND, UTAH	0.11
	LOAM 20% WATER	0.11

TABLE 3. SENSITIVITY CHARACTERISTICS OF THEMATIC MAPPER

CHANNEL	SPECTRAL WIDTH	SNR FOR LOW LEVEL INPUT[a]	NORMALIZED LOW LEVEL IMPUT FROM SIMULATION[b] ($W\ m^{-2}\ sr^{-1}\ \mu m^{-1}$)	NORMALIZED rms NOISE, σ_n
1	0.45-0.52	32	1.58	.049
2	0.52-0.60	35	1.00	.029
3	0.63-0.69	26	.60	.023
4	0.76-0.90	32	.28	.009
5	1.55-1.75	13	.16	.012

[a]Specified in Ref. 24 as $\rho = 0.01$ and $\theta_o = 70^o$ for bands 1 to 4, and $\rho = 0.02$ and $\theta_o = 10^o$ for band 5.

[b]Mean value for visual range V = 55 km.

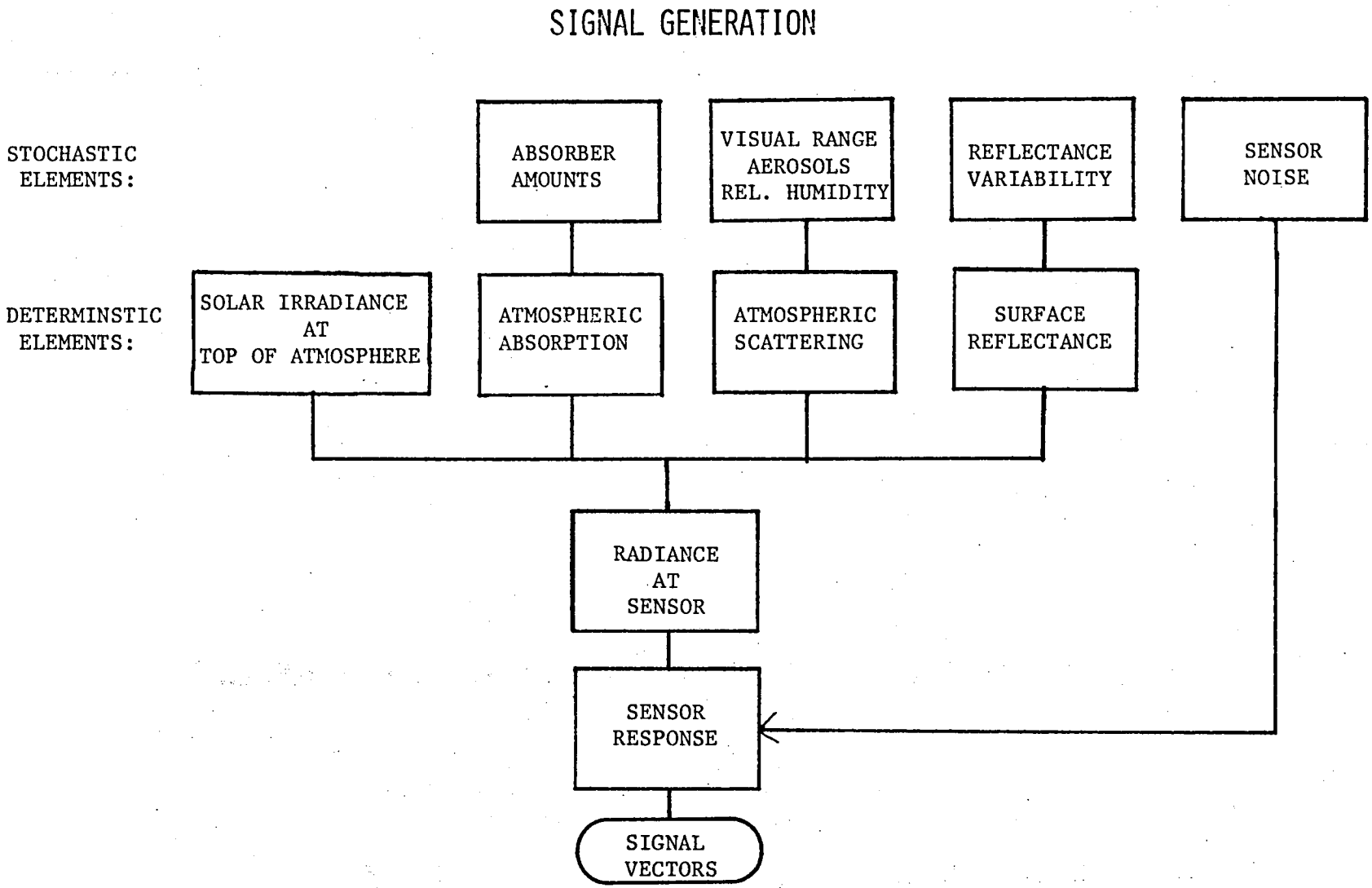

FIGURE 1. SCHEMATIC OF SIGNAL GENERATION MODEL

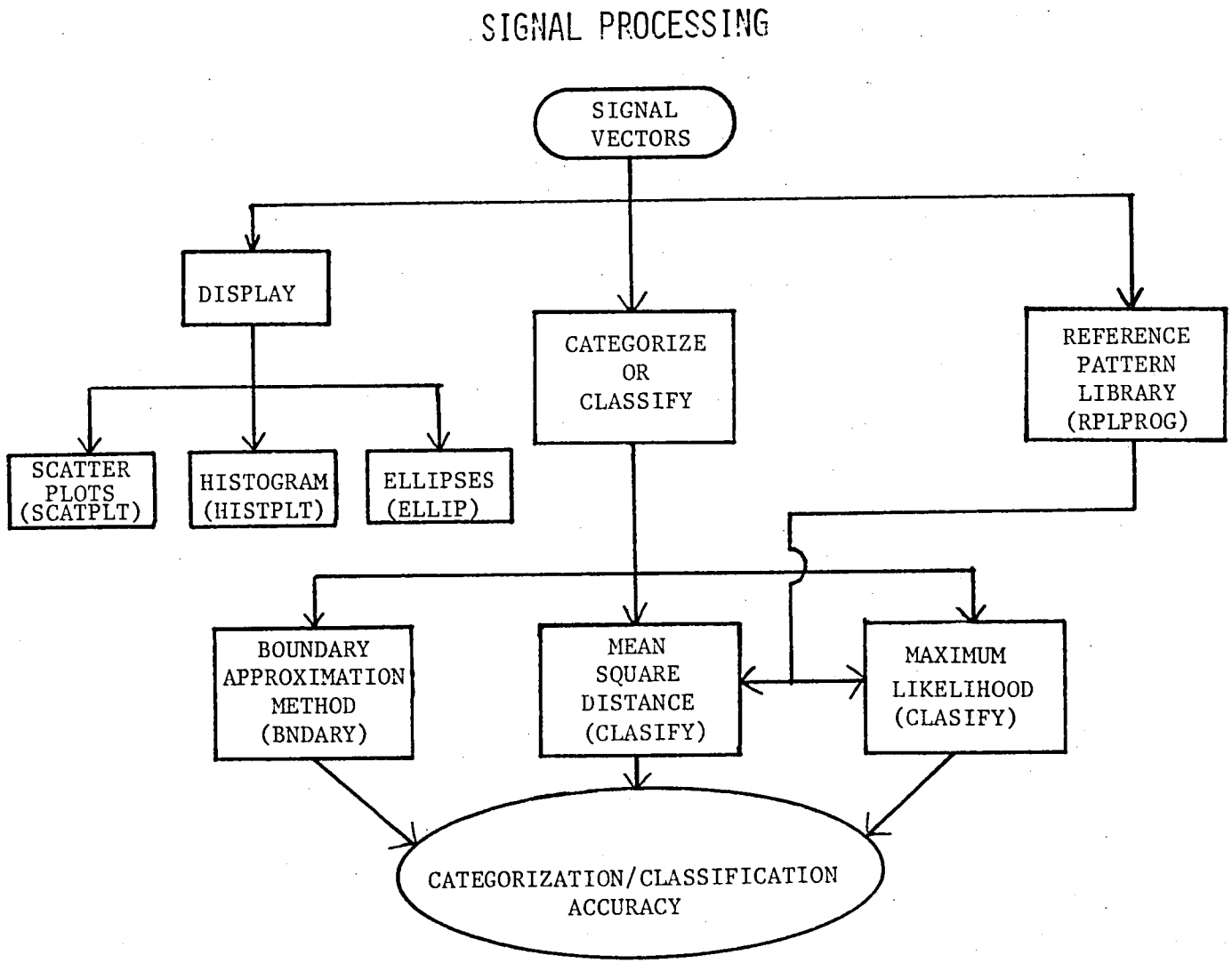

FIGURE 2. SCHEMATIC OF SIGNAL PROCESSING OPTIONS (PROGRAM NAMES IN PARENTHESES)

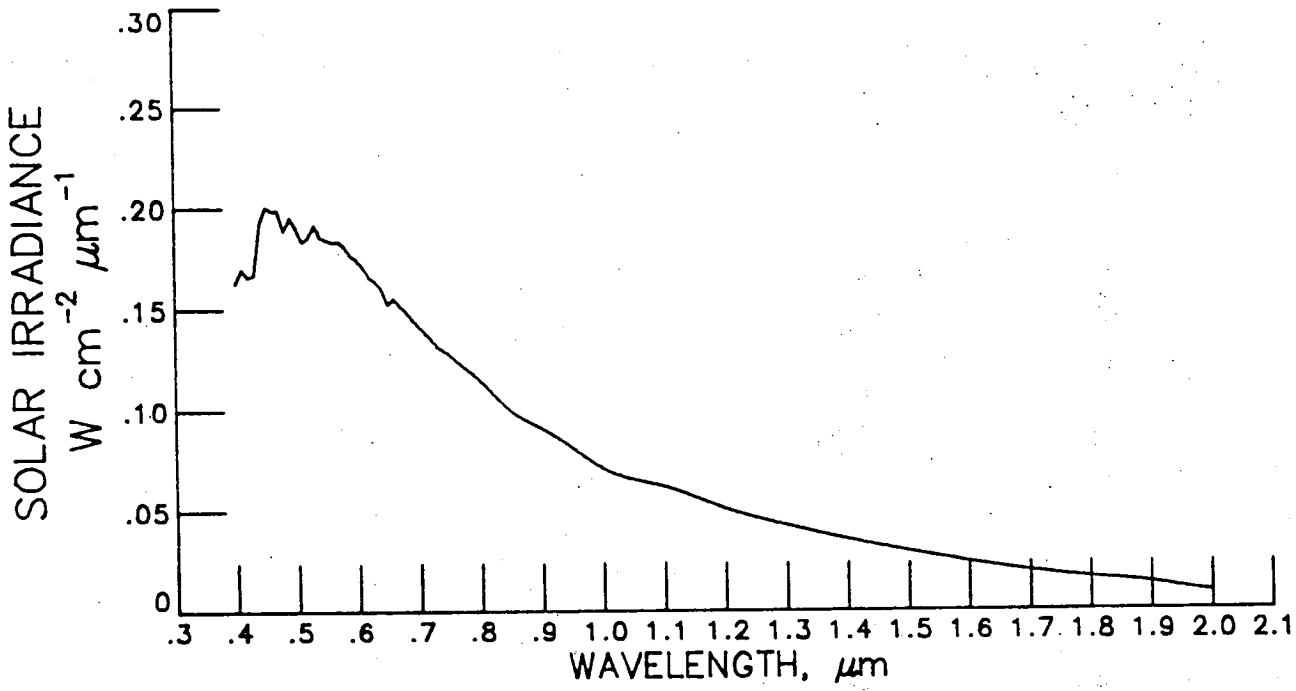

FIGURE 3. SOLAR IRRADIANCE AT TOP OF ATMOSPHERE

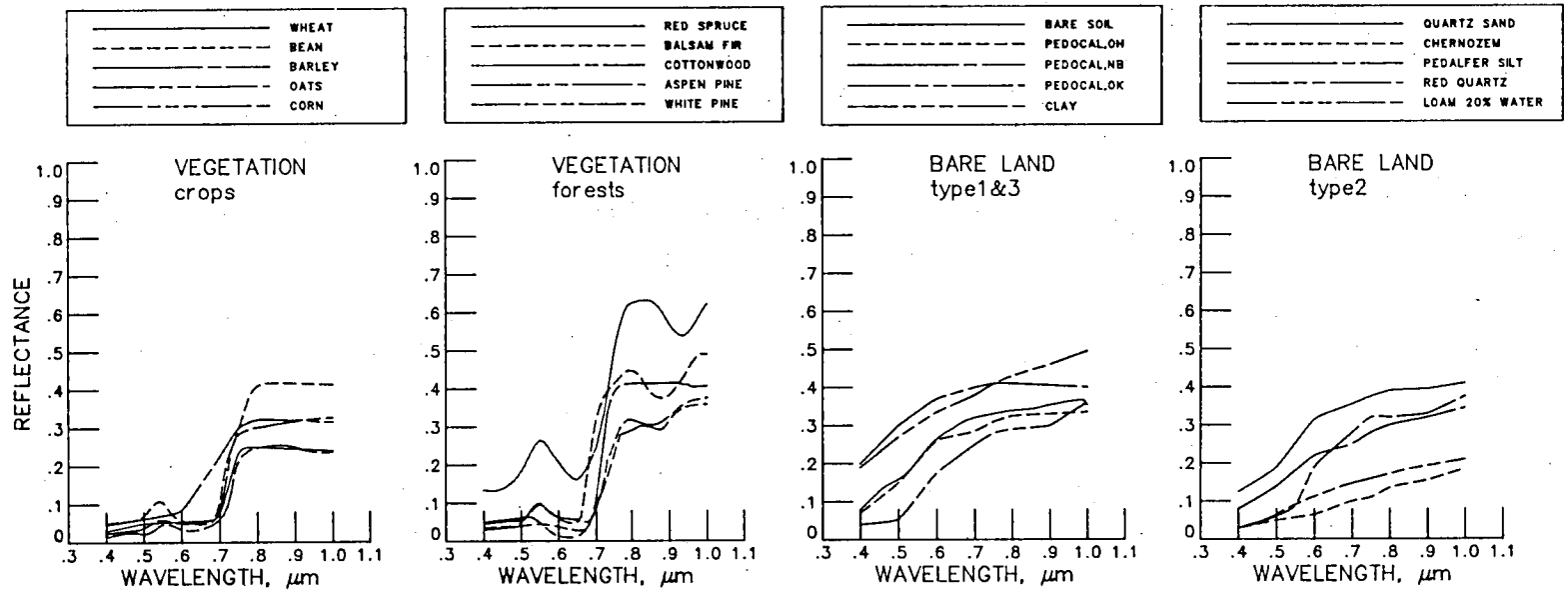

FIGURE 4. MEAN SPECTRAL REFLECTANCES

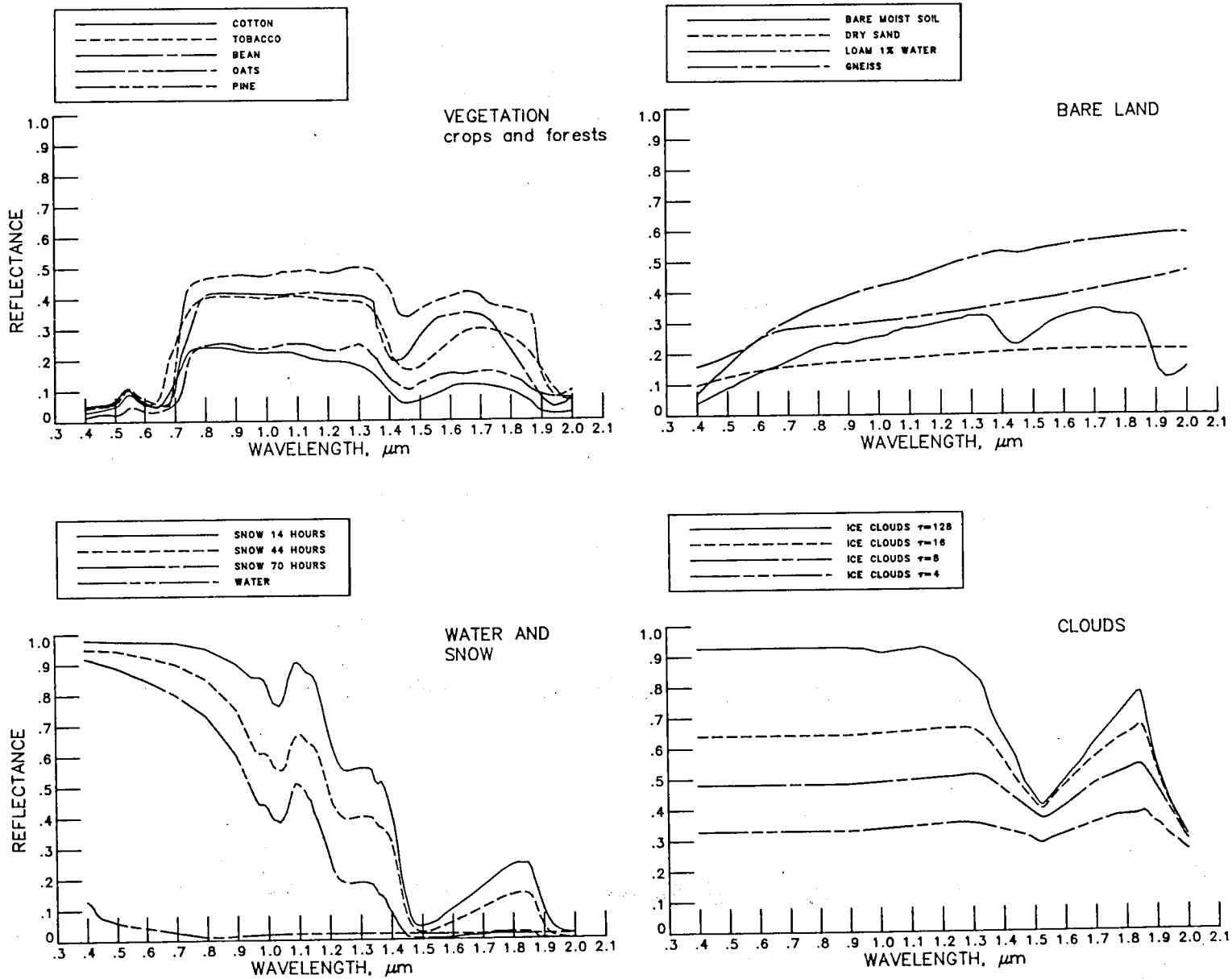

FIGURE 4. MEAN SPECTRAL REFLECTANCES (CONCLUDED)

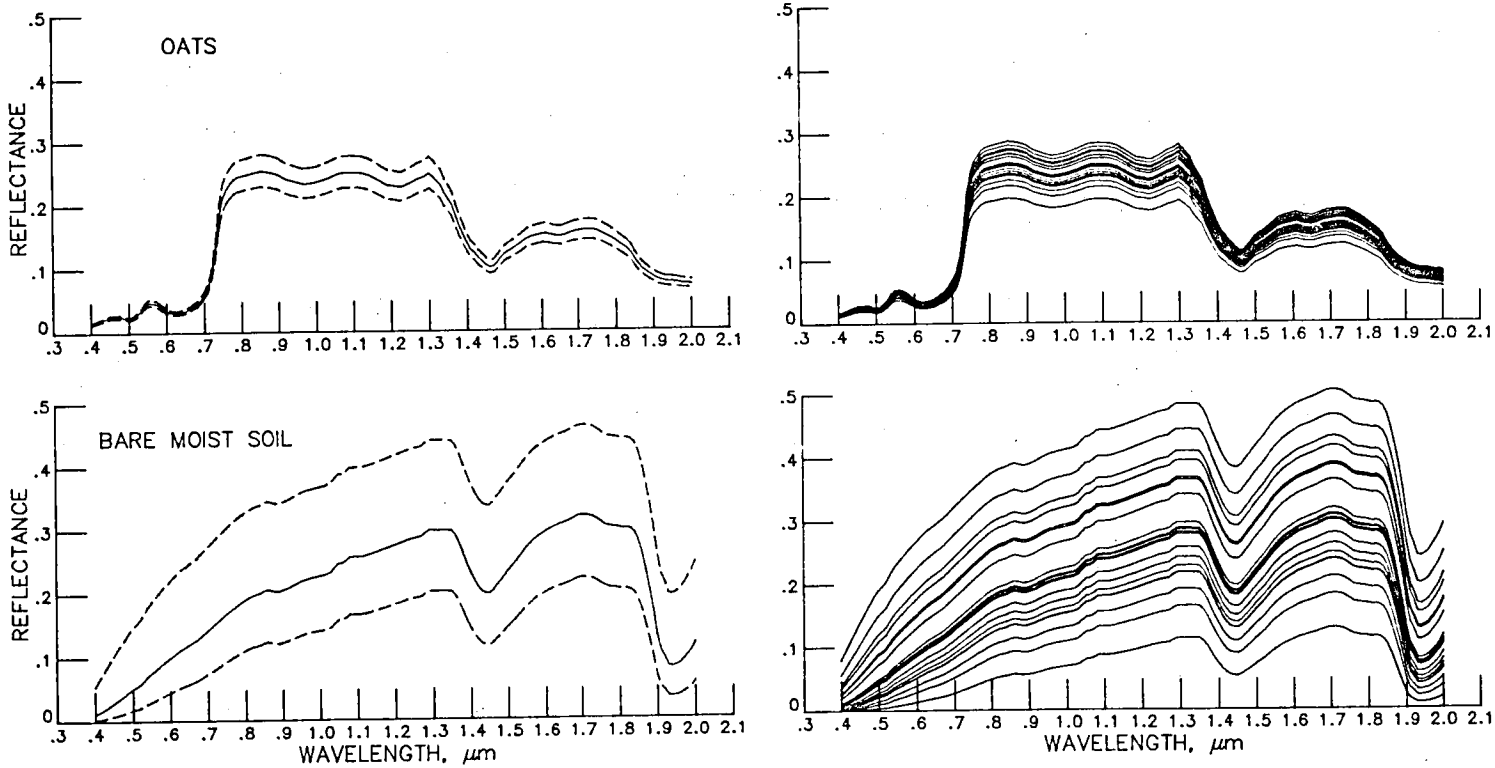

(a) Average reflectance and standard deviation.

(b) Typical realization of variability.

FIGURE 5. SIMULATED SPECTRAL REFLECTANCE VARIABILITY FOR TWO TARGETS

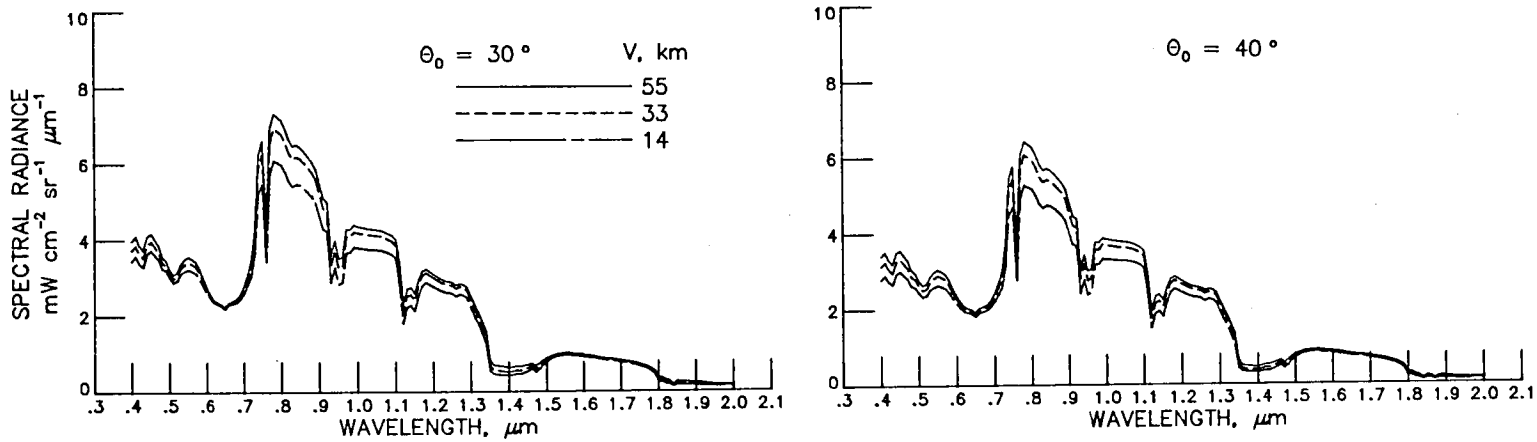

FIGURE 6. MEAN SPECTRAL RADIANCES INCIDENT ON REMOTE SENSOR FOR TWO SOLAR INCIDENCE ANGLES, θ_o, AND THREE VISUAL RANGES, V, USING OATS AS TARGET AND BARE MOIST SOIL AS BACKGROUND

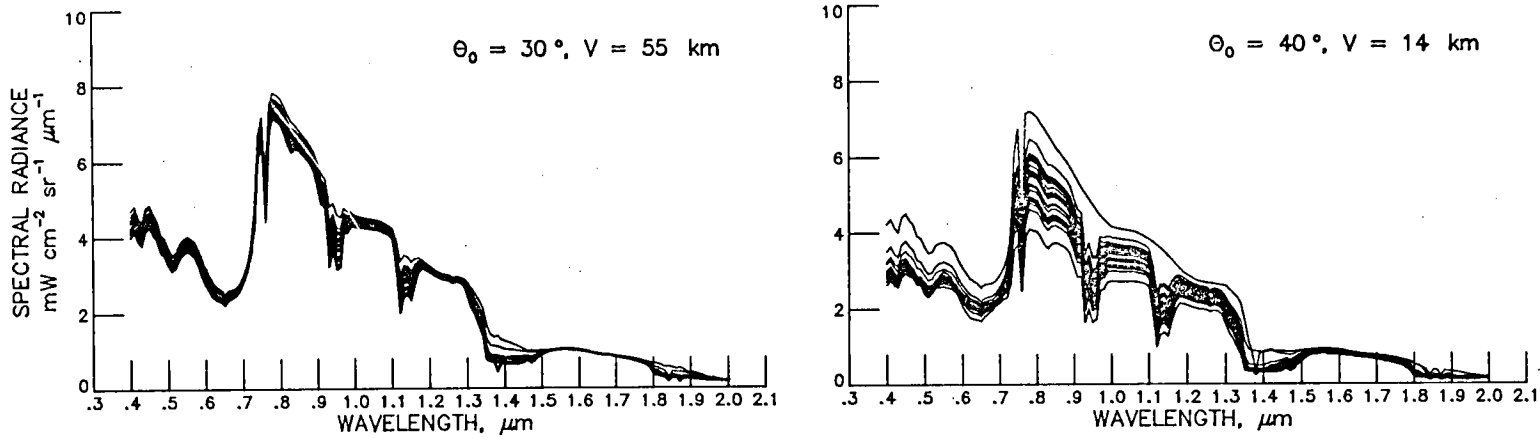

(a) Accounting for the effects of atmospheric variability only.

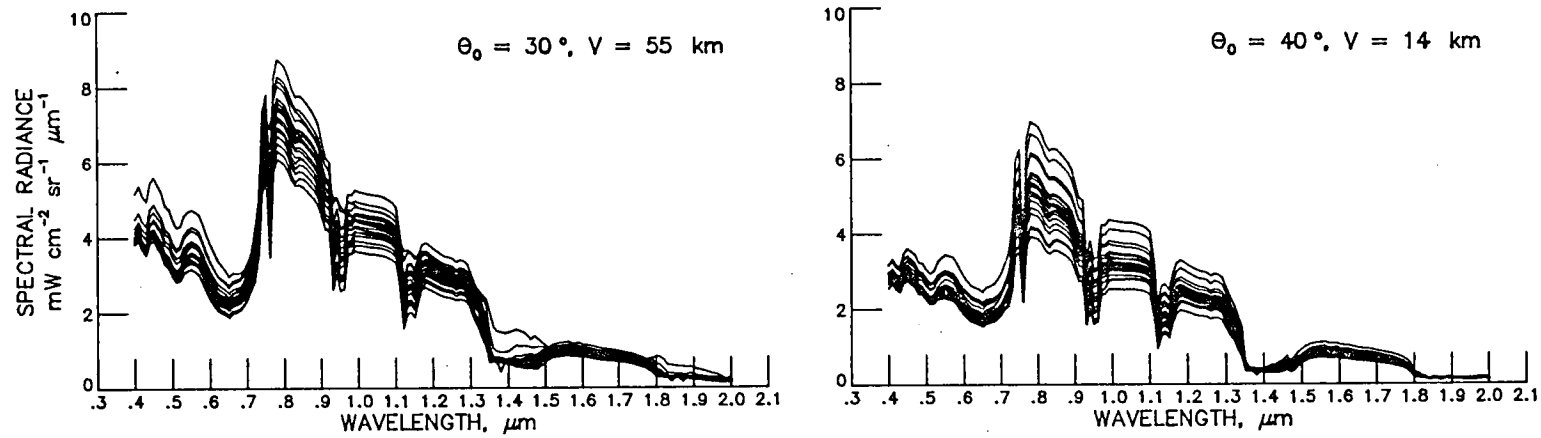

(b) Accounting for the effects of both atmospheric and surface variability.

FIGURE 7. TYPICAL REALIZATIONS OF SPECTRAL RADIANCE VARIABILITY FOR TWO VIEWING CONDITIONS, USING OATS AS TARGET AND BARE MOIST SOIL AS BACKGROUND

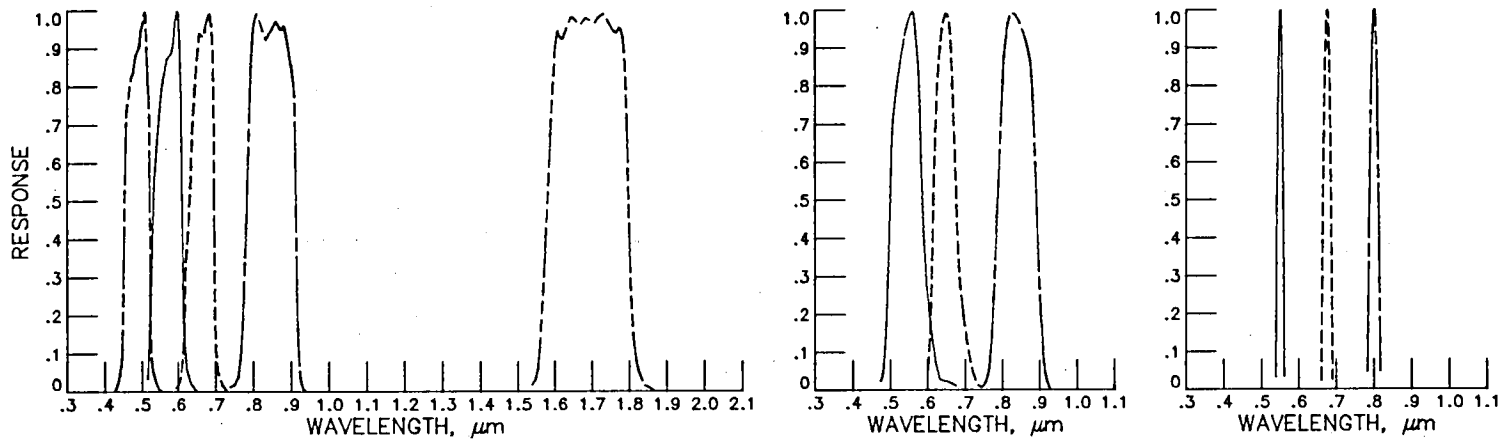

FIGURE 8. SIMULATED SPECTRAL SENSOR RESPONSES

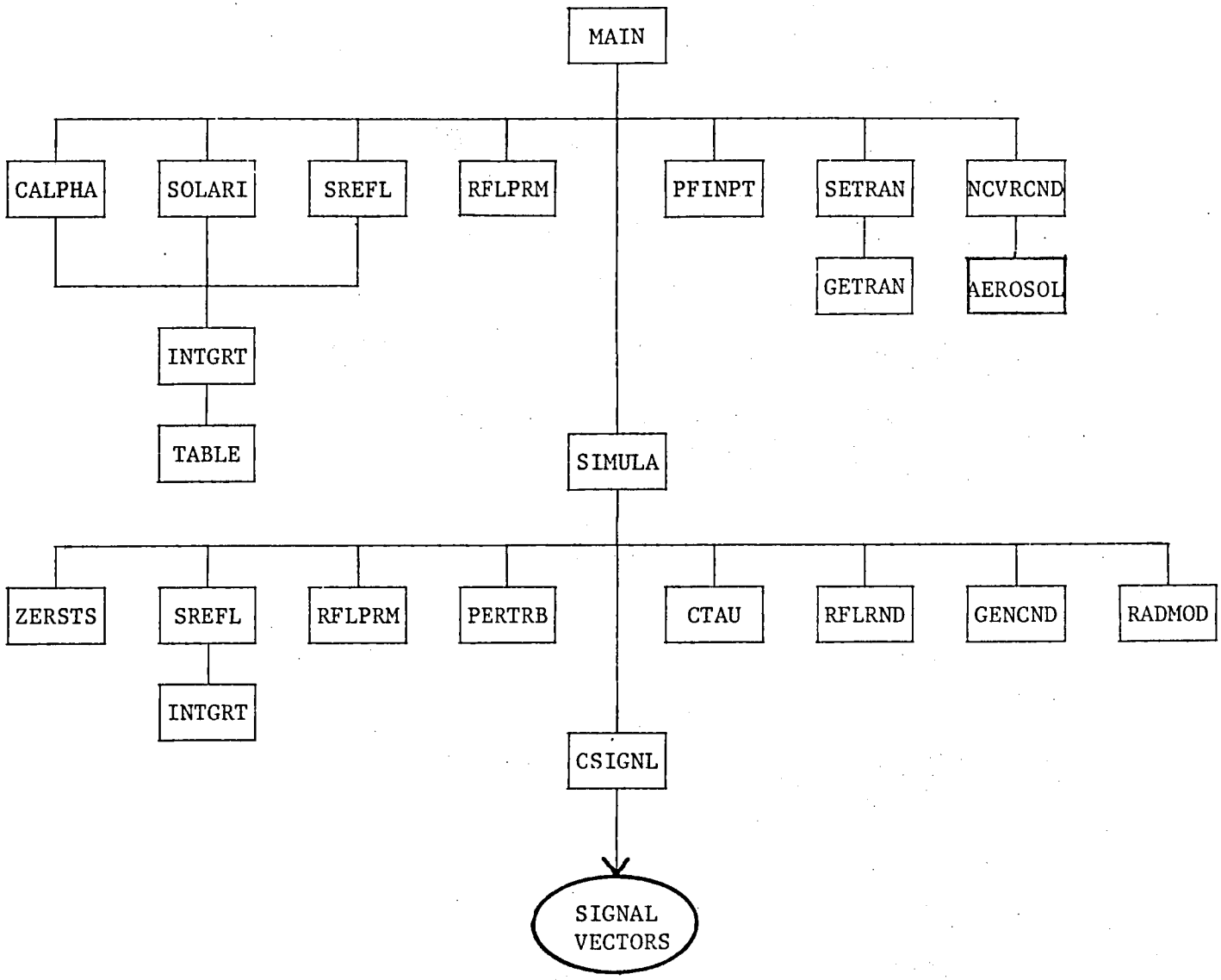

FIGURE 9. STIMULA PROGRAM STRUCTURE

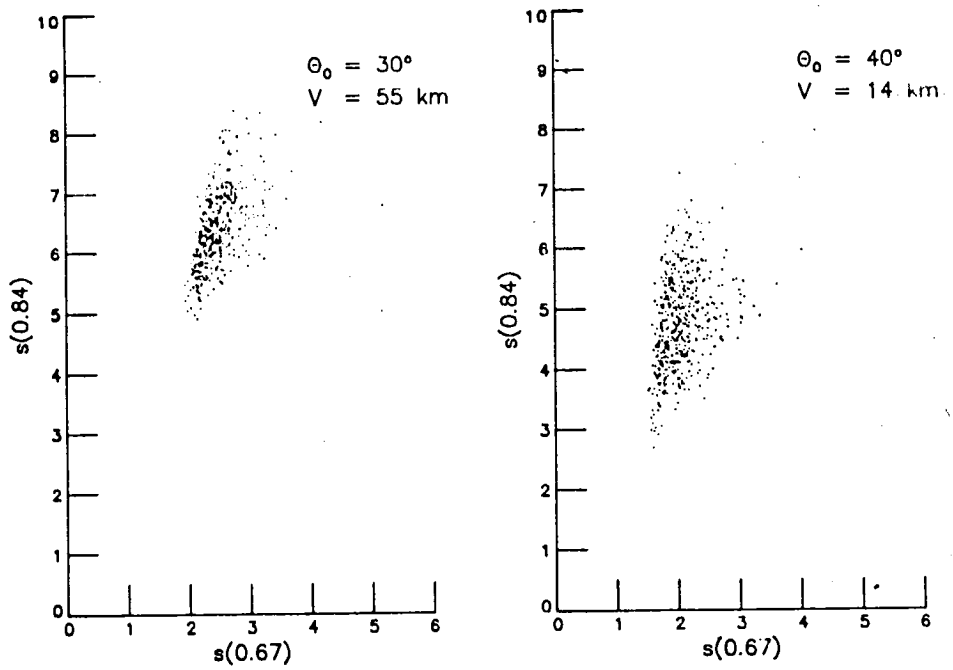

FIGURE 10. SIGNAL SCATTER PLOT FOR TWO TM CHANNELS, USING OATS AS TARGET AND BARE MOIST SOIL AS BACKGROUND

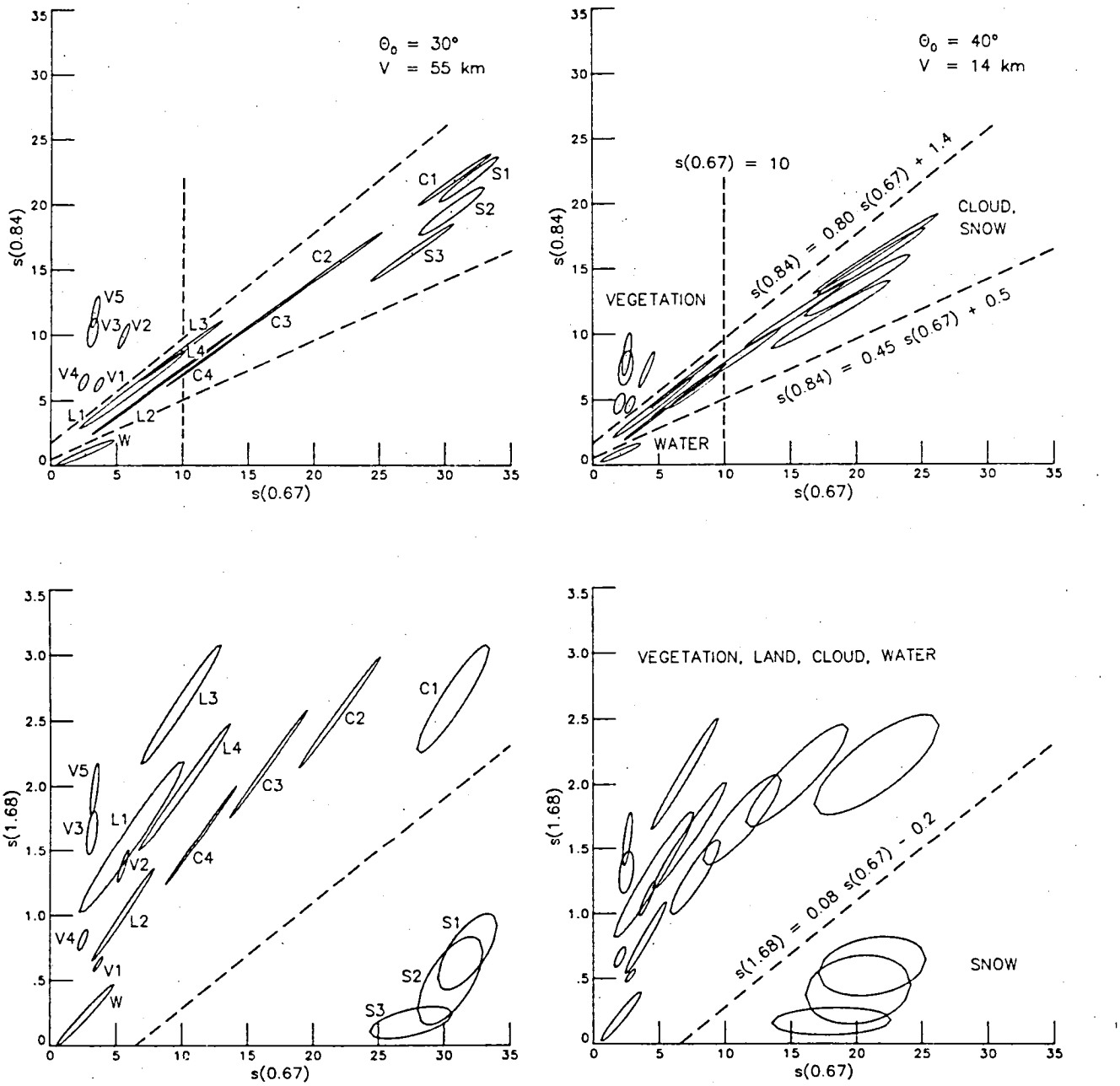

FIGURE 11. SIGNAL COVARIANCE CONTOURS FOR THREE TM CHANNELS, USING THE SUBSTANCES LISTED IN TABLE 2(a) AS TARGETS AND BARE MOIST SOIL AS BACKGROUND. THE BOUNDARIES (DASHED LINES) ARE USED TO DISTINGUISH BETWEEN THE CATEGORIES VEGETATION, BARE LAND, WATER, SNOW AND CLOUD.

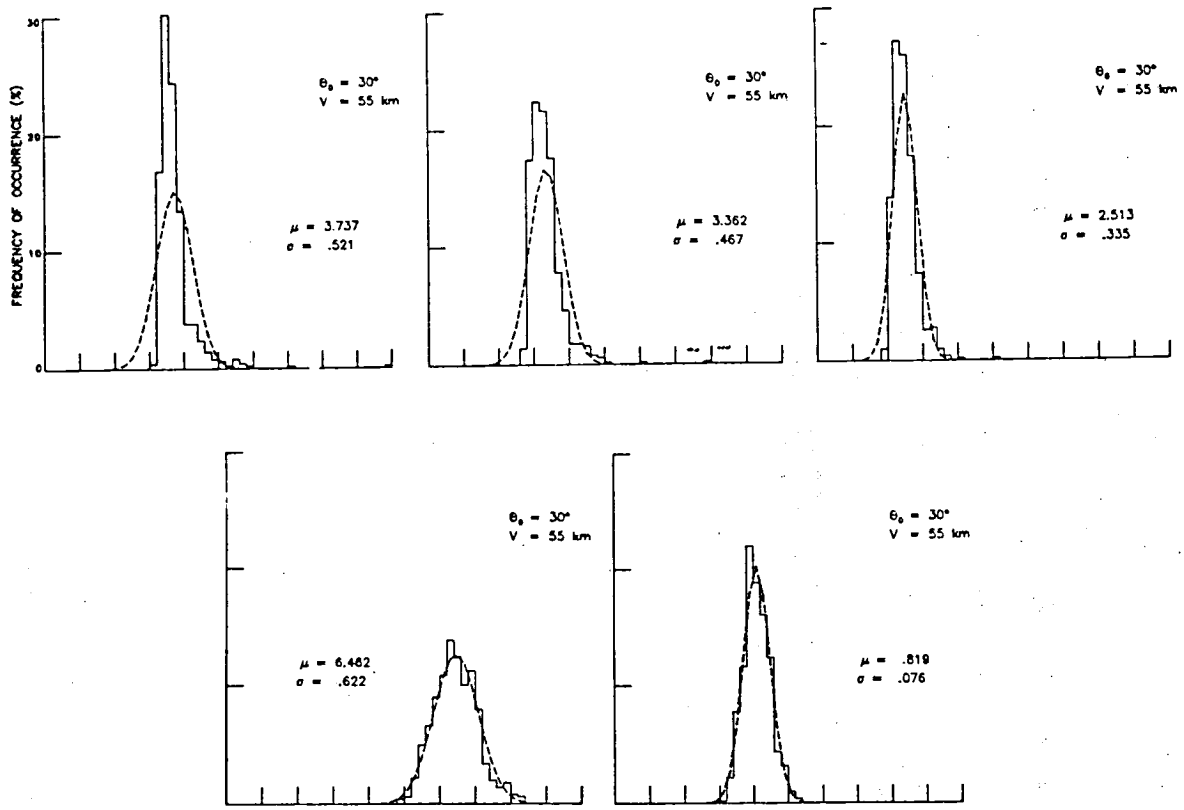

FIGURE 12. TM SIGNAL HISTOGRAM (SOLID) AND "EQUIVALENT" GAUSSIAN DISTRIBUTION (DASHED) WITH EQUAL MEAN AND VARIANCE, USING OATS AS TARGET AND BARE MOIST SOIL AS BACKGROUND. THE CORRESPONDING RADIANCE VARIABILITY IS ILLUSTRATED IN FIG. 7(b).

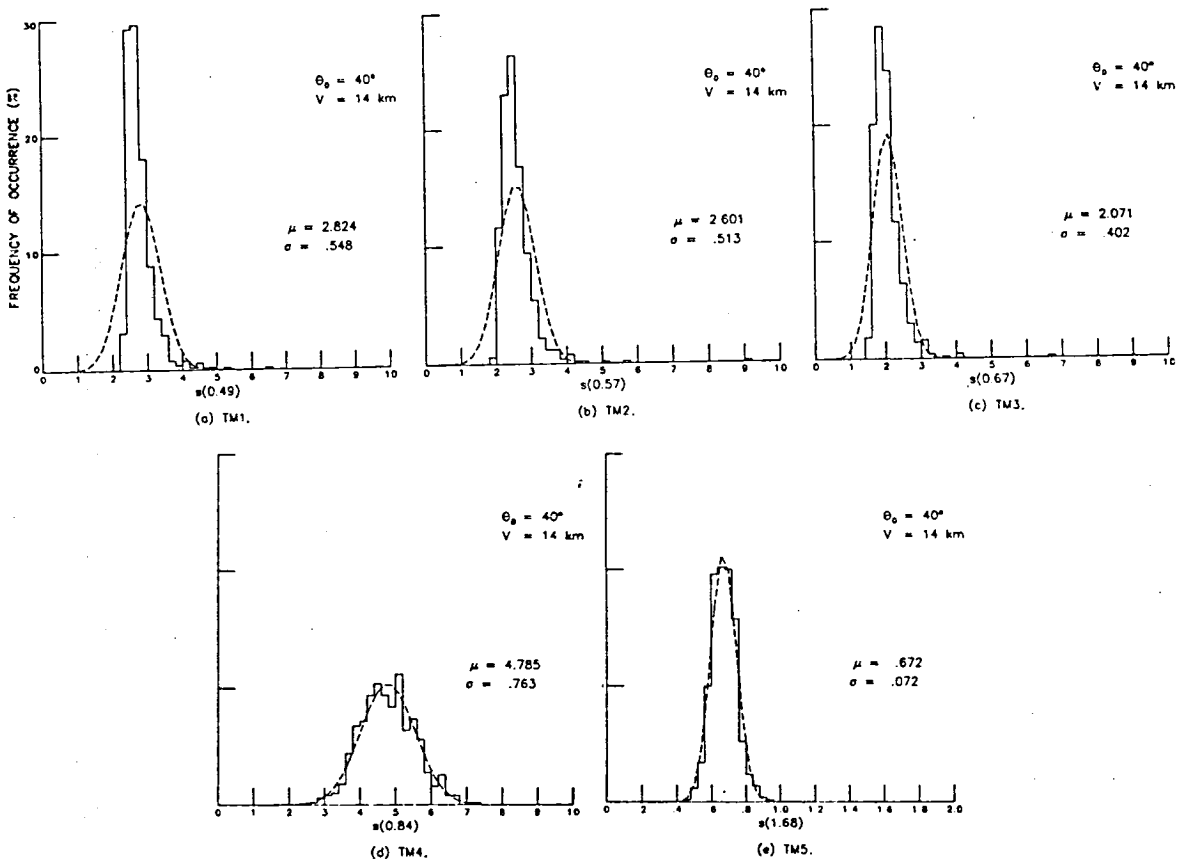

FIGURE 12. TM SIGNAL HISTOGRAM (SOLID) AND "EQUIVALENT" GAUSSIAN DISTRIBUTION (DASHED) WITH EQUAL MEAN AND VARIANCE, USING OATS AS TARGET AND BARE MOIST SOIL AS BACKGROUND. THE CORRESPONDING RADIANCE VARIABILITY IS ILLUSTRATED IN FIG. 7(b) (CONCLUDED).

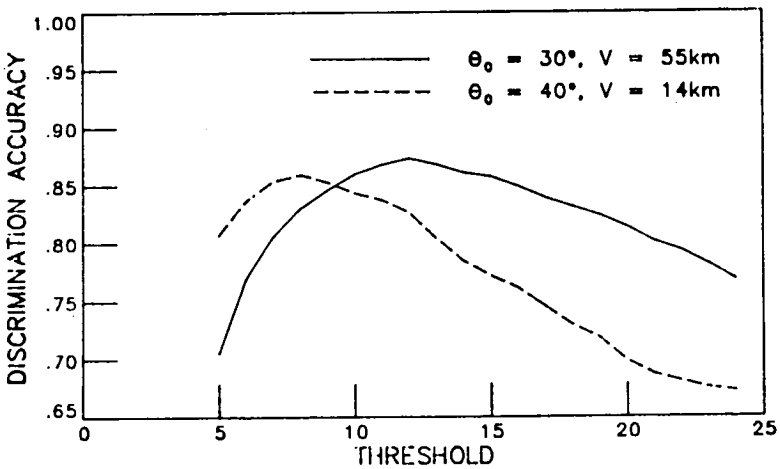

Discrimination between vegetation/land/water and snow/cloud for unratioed signals.

FIGURE 13. DISCRIMINATION ACCURACY VERSUS THRESHOLD BOUNDARY BETWEEN GROUPS OF CATEGORIES, USING THE TM CHANNEL LOCATED AT 0.67 μm

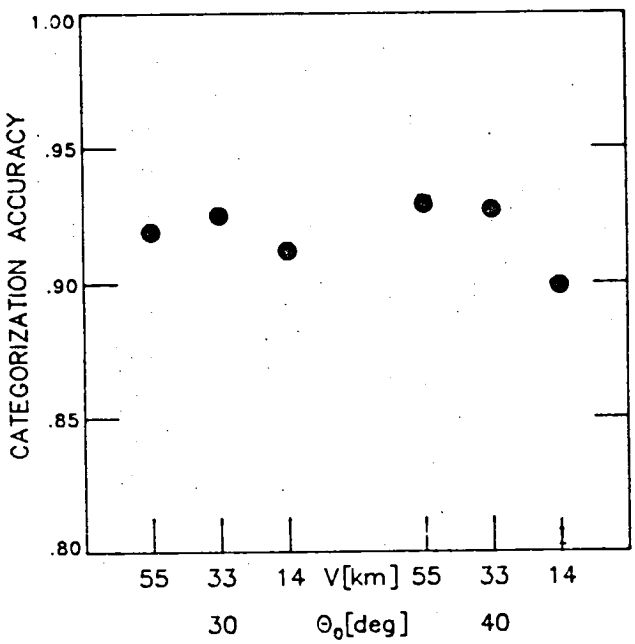

FIGURE 14. FEATURE CATEGORIZATION ACCURACY FOR SEVERAL IMAGING CONDITIONS USING THE TM CHANNELS LOCATED AT 0.67, 0.84, AND 1.68 μm

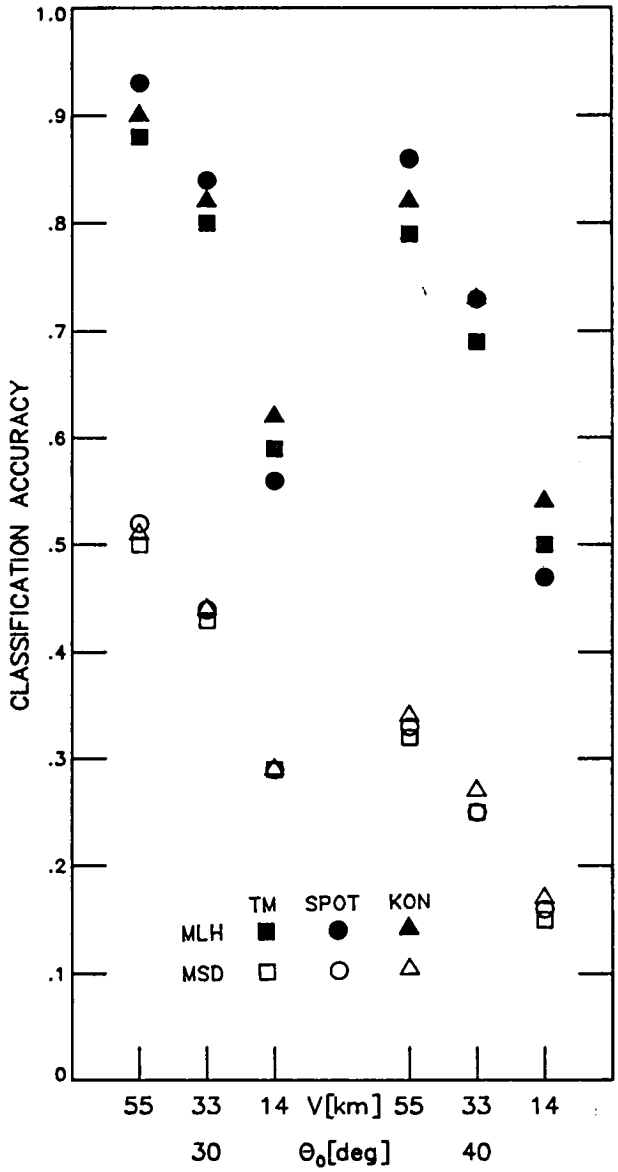

FIGURE 15. FEATURE IDENTIFICATION ACCURACY FOR SEVERAL IMAGING CONDITIONS, USING THE THREE TM, SPOT, AND KON RESPONSES LOCATED AT NEARLY THE SAME WAVELENGTHS WITH EITHER MLH OR MSD CLASSIFICATION OF UNRATIOED SIGNALS.

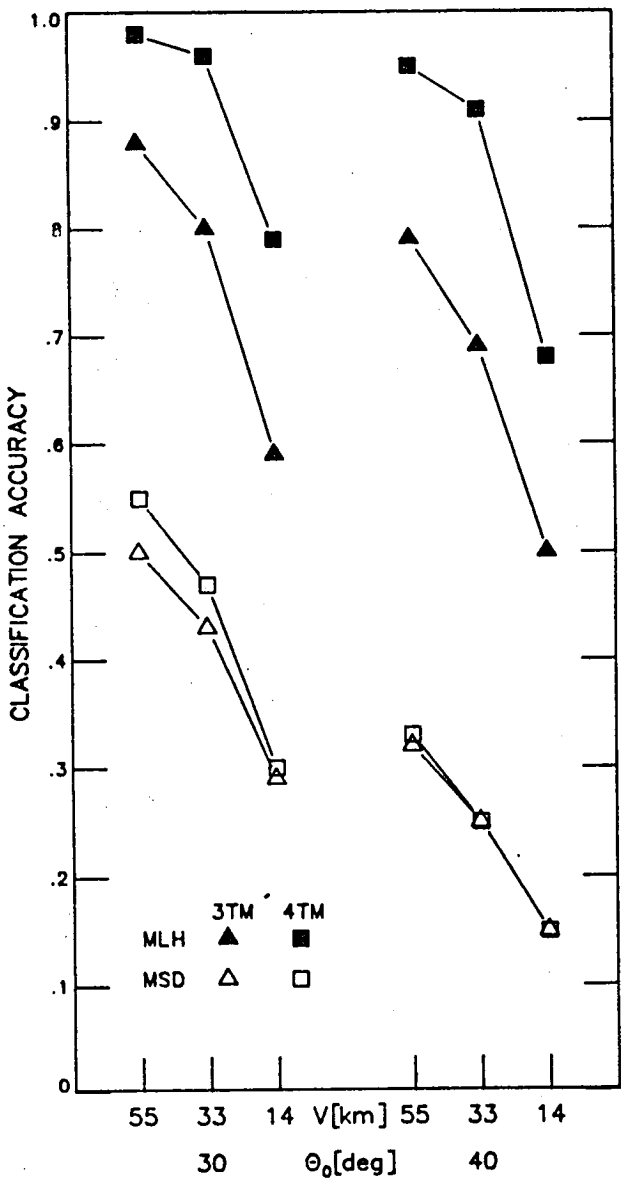

MLH and MSD classification of signals.

FIGURE 16. FEATURE IDENTIFICATION ACCURACY FOR SEVERAL IMAGING CONDITIONS USING EITHER THREE OR FOUR TM CHANNELS WITH EITHER MLH OR MSD CLASSIFICATION OF SIGNALS

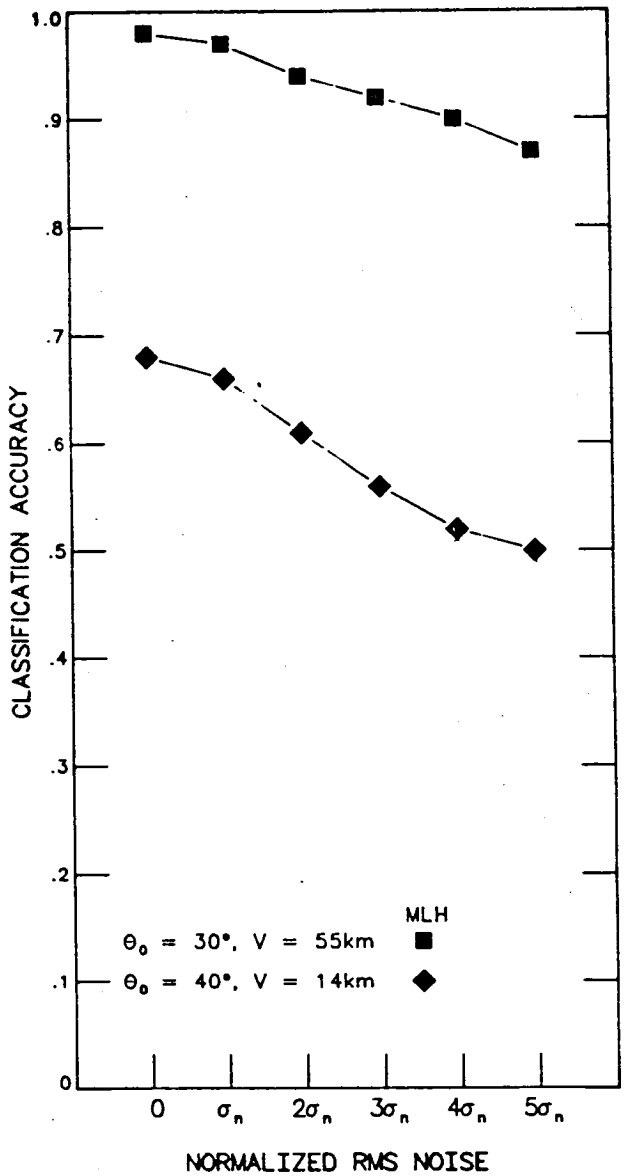

FIGURE 17. FEATURE IDENTIFICATION ACCURACY FOR SEVERAL SENSOR NOISE LEVELS AND TWO IMAGING CONDITIONS, USING FOUR TM CHANNELS WITH MLH CLASSIFICATION OF SIGNALS

1. Report No.	2. Government Accession No.	3. Recipient's Catalog No.
NASA CR-172393		

4. Title and Subtitle	5. Report Date
A SIMULATION OF REMOTE SENSOR SYSTEMS AND DATA PROCESSING ALGORITHMS FOR SPECTRAL FEATURE CLASSIFICATION	JULY 1984
	6. Performing Organization Code

7. Author(s)	8. Performing Organization Report No.
ROBERT F. ARDUINI, R. MARTIN AHERRON, RICHARD W. SAMMS	FR 683110
	10. Work Unit No.

9. Performing Organization Name and Address	11. Contract or Grant No.
INFORMATION & CONTROL SYSTEMS, INCORPORATED 28 RESEARCH DRIVE HAMPTON, VA 23666	NAS1-16870
	13. Type of Report and Period Covered
12. Sponsoring Agency Name and Address	CONTRACTOR REPORT
NATIONAL AERONAUTICS AND SPACE ADMINISTRATION WASHINGTON, DC 20546	14. Sponsoring Agency Code
	506-58-13-11

15. Supplementary Notes

NASA LANGLEY TECHNICAL MONITOR: RICHARD E. DAVIS
FINAL REPORT

16. Abstract

A computational model of the deterministic and stochastic processes involved in multispectral remote sensing has been designed to evaluate the performance of sensor systems and data processing algorithms for spectral feature classification. Accuracy in distinguishing between categories of surfaces or between specific types is developed as a means to compare sensor systems and data processing algorithms. The model allows studies to be made of the effects of variability of the atmosphere and of surface reflectance, as well as the effects of channel selection and sensor noise. Examples of these effects are shown.

17. Key Words (Suggested by Author(s))	18. Distribution Statement
Multispectral Sensor; Remote Sensor; Smart Sensor; Spectral Responses; Classification Algorithms; Feature Classification; Spectral Reflectances.	Unclassified-Unlimited Subject Category - 35

19. Security Classif. (of this report)	20. Security Classif. (of this page)	21. No. of Pages	22. Price
Unclassified	Unclassified	54	A04

For sale by the National Technical Information Service, Springfield, Virginia 22161